ChemPubSoc Europe

DOI: 10.1002/cbic.201800737

CHEMBIOCHEM Full Papers

Modulating Protein–Protein Interactions with Visible-Light-Responsive Peptide Backbone Photoswitches

Lea Albert,[a] Alberto Peñalver,[a] Nemanja Djokovic,[b] Laura Werel,[a] Malte Hoffarth,[a] Dusan Ruzic,[b] Jing Xu,[c] Lars-Oliver Essen,[a] Katarina Nikolic,[b] Yali Dou,[c] and Olalla Vázquez*[a]

Life relies on a myriad of carefully orchestrated processes, in which proteins and their direct interplay ultimately determine cellular function and disease. Modulation of this complex crosstalk has recently attracted attention, even as a novel therapeutic strategy. Herein, we describe the synthesis and characterization of two visible-light-responsive peptide backbone photoswitches based on azobenzene derivatives, to exert optical control over protein–protein interactions (PPI). The novel peptidomimetics undergo fast and reversible isomerization with low photochemical fatigue under alternatively blue-/green-light irradiation cycles. Both bind in the nanomolar range to the protein of interest. Importantly, the best peptidomimetic displays a clear difference between isomers in its protein-binding capacity and, in turn, in its potential to inhibit enzymatic activity through PPI disruption. In addition, crystal structure determination, docking and molecular dynamics calculations allow a molecular interpretation and open up new avenues in the design and synthesis of future photoswitchable PPI modulators.

Introduction

Proteins play a key role in the regulation of cellular behavior and are, therefore, also involved in the development of diseases. Despite the fact that some proteins perform their functions independently, the reality is that most of them are integrated in complex dynamic networks ruled by protein–protein interactions (PPIs).[1] This crosstalk controls both protein production and activity, as well as signal transduction and metabolic pathways. Therefore, breaking the molecular code associated with PPIs will pave the way for on-demand modulation of functional outcomes capable of affecting pathogenic mechanisms. Historically, PPIs with relatively large buried interfaces have been considered "undruggable" targets.[2] However, recent years have witnessed an outstanding success in targeting PPIs through many different approaches, such as small-molecule derivatives, recombinant proteins, antibodies, and peptides.[3] In particular, the use of peptidomimetics has acquired increasing relevance because they not only retain the advantages of peptides, but also overcome their intrinsic limitations to provide new features.[4] For example, by grafting a light-driven molecular transducer onto a peptide scaffold, spatiotemporal resolution could be achievable to circumvent the common off-target effects in therapy.

Azobenzenes[5] are by far the most extensively used photoswitches in the context of photopharmacology.[6] However, their *trans*→*cis* isomerization wavelength at 366 nm is not ideal for in vivo applications and, furthermore, this photoisomerization is not complete. Therefore, in the last few years, there has been great interest in developing visible-light-shifting azobenzenes to overcome such limitations.[7] Among these second-generation compounds, the cyclic azobenzene (cAzo) 5,6-dihydrodibenzo[*c*,*g*][1,2]diazocine is a very interesting one.[8] The C2 bridge produces a highly twisted *trans* isomer that is less stable than the *cis* conformation; this contrasts with the situation in "normal" azobenzenes. *p*-Acetoamido substituents in the cAzo core enable slightly red-shifted isomerization wavelengths.[9] More importantly, the separation of the n→π* transition is large (85 nm), so that selective irradiation is possible. The same behavior was also observed with tetra-*ortho*-substituted azobenzenes.[10] In particular, the group of Hecht has optimized the properties of classical azobenzenes by introducing σ-electron-withdrawing fluorine atoms in these positions, which leads to visible-light switches with high photoconversions and very long lived *cis* isomers.[7c] Since this contribution, tetra-*ortho*-fluoroazobenzenes have been mainly used in materials science,[11] and their applications in a biological context are scarce.[12] Along these lines, there have been only a

[a] L. Albert, A. Peñalver, L. Werel, M. Hoffarth, Prof. Dr. L.-O. Essen, Prof. Dr. O. Vázquez
Fachbereich Chemie, Philipps-Universität Marburg
Hans-Meerwein-Strasse 4, 35043, Marburg (Germany)
E-mail: olalla.vazquez@staff.uni-marburg.de

[b] N. Djokovic, D. Ruzic, K. Nikolic
Department of Pharmaceutical Chemistry
Faculty of Pharmacy, University of Belgrade
450 Vojvode Stepe, 11000 Belgrade (Serbia)

[c] Dr. J. Xu, Prof. Dr. Y. Dou
Department of Pathology, University of Michigan
Ann Arbor, MI 48109 (USA)

Supporting information and the ORCID identification numbers for the authors of this article can be found under https://doi.org/10.1002/cbic.201800737.

This article is part of the young researchers' issue. To view the complete issue, visit http://chembiochem.org/chembiotalents

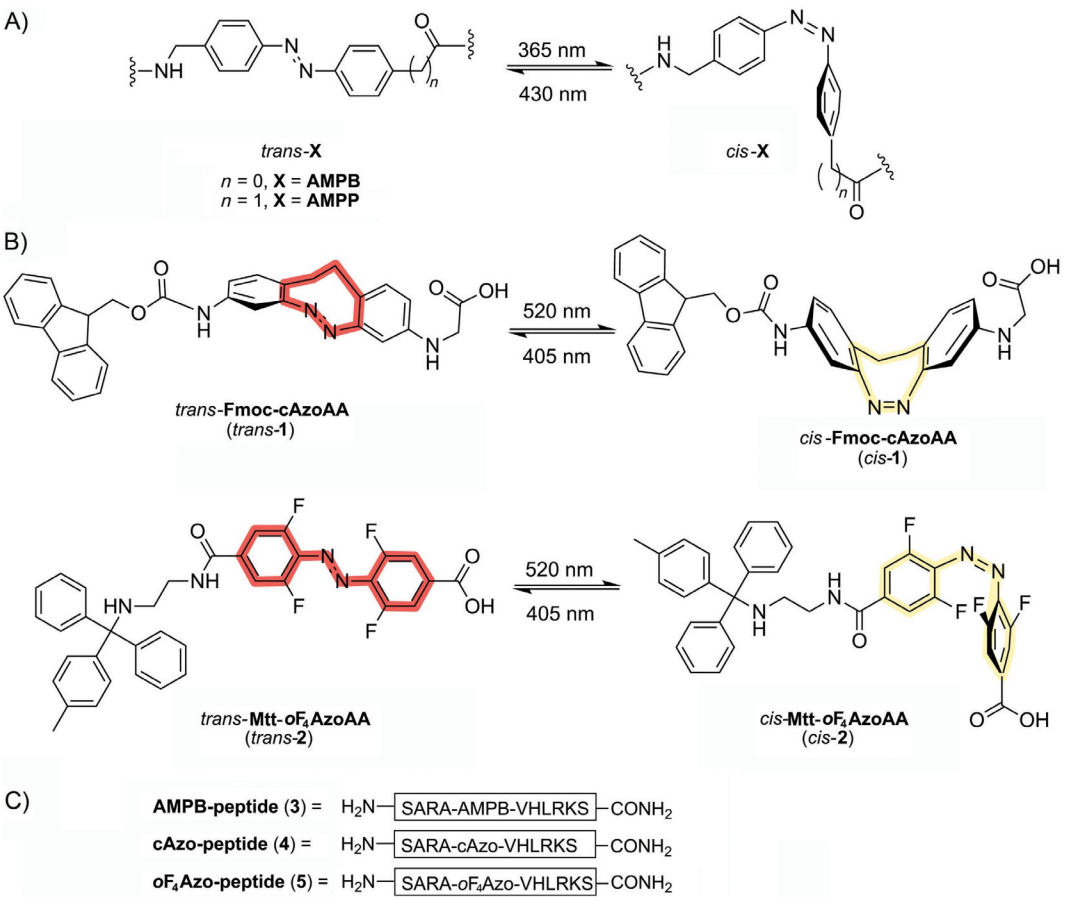

Scheme 1. A) Previously reported light-responsive peptide backbone photoswitches. B) Structure and isomerization of the new visible-light photoswitchable amino acids reported herein: Fmoc-cAzoAA (**1**) and Mtt-oF4AzoAA (**2**). C) Former photoswitchable peptidomimetic used for MLL1-WDR5 PPI disruption (**3**) and new ones reported herein, which contain visible-light-responsive peptide backbone photoswitches.

few cAzo derivatives used to modulate DNA hybridization[13] and to control the helical conformation of peptides.[9b]

Regarding azo-containing proteins and peptides, the strategies employed to introduce red-shifted azobenzenes are mainly restricted to cysteine-reactive tethered derivatives as side-chain crosslinkers[14] and genetic encoding of the azobenzene amino acids.[15] However, to the best of our knowledge, the direct inclusion of the azobenzene unit into peptide backbones is still limited to unsubstituted derivatives as classic fluorenylmethyloxycarbonyl (Fmoc)-building blocks: [3-(3-aminomethyl)phenylazo]phenylacetic acid (AMPP),[16] (4-aminomethyl)phenylazobenzoic acid (AMPB),[17] and commercially available Fmoc-L-phenylalanine-4′-azobenzene.

Herein, we describe the synthesis and characterization of two novel visible-light photocontrollable amino acids based on the previous derivatives of Bléger et al.[18] and Siewertsen et al.[8] to be grafted onto a peptide scaffold. As our group has recently reported the possibility of externally controlling leukemia cell proliferation by disrupting the essential epigenetic PPI MLL1-WDR5, with photoswitchable azobenzene-containing peptides,[19] we use this biological system to study its potential as novel PPI modulators. So far, to the best of our knowledge, no attempts to incorporate either tetra-*ortho*-fluoroazobenzenes or cyclic derivatives into peptide backbones have been reported. Exploring second-generation azobenzenes as visible-light-responsive peptide backbone photoswitches will complement information on systems in which the photoswitches are attached to the N terminus of the peptide sequence, or on the side chain of an amino acid as crosslinkers. Furthermore, it will contribute to gaining an insight into the design of peptidomimetics (Scheme 1).

Olalla Vázquez obtained her PhD in chemistry under the supervision of Profs. José Luis Mascareñas and Eugenio Vázquez, at Universidade de Santiago de Compostela (2010) working on synthetic transcription factors and fluorescent DNA binders. She was a visiting PhD student at Harvard University in Prof. Verdine' group (2006) and at Humboldt Universität zu Berlin with Prof. Seitz (2008). In 2011 she received a Marie Curie postdoctoral fellowship to explore RNA template-directed reactions in the context of cancer therapy. She is currently Assistant Professor at Philipps-Universität Marburg. Her research focuses on developing optochemical tools to control and understand biological processes at molecular level.

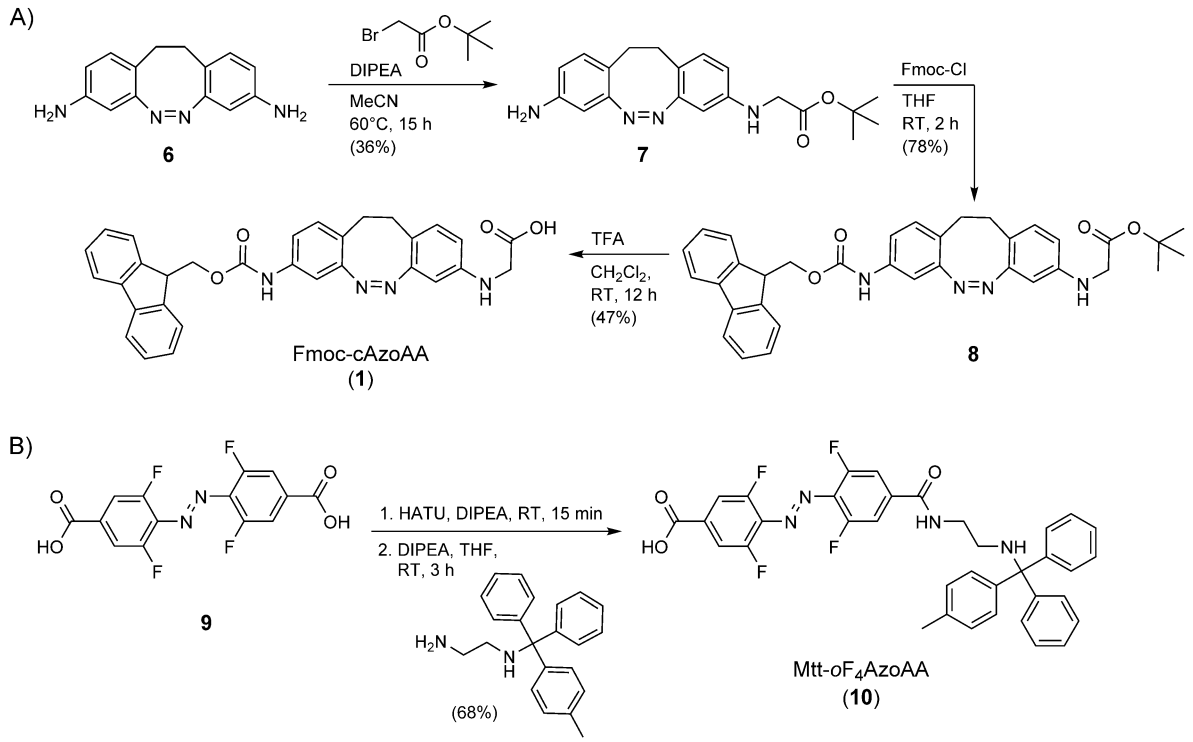

Scheme 2. Synthetic routes to the visible-light photoswitchable amino acids: A) Fmoc-cAzoAA (**1**) and B) Mtt-oF_4AzoAA (**2**). TFA: trifluoroacetic acid, HATU: 1-[bis(dimethylamino)methylene]-1*H*-1,2,3-triazolo[4,5-*b*]pyridinium 3-oxid hexafluorophosphate. DIPEA: *N*,*N*-diisopropylethylamine

Results and Discussion

Synthesis of photoswitchable building blocks and inclusion into the peptide backbone

To simplify the synthetic work, even at the expense of moderate yields, we followed previous procedures of azobenzene cyclization[9] and obtained compound **6** (Scheme 2). Afterwards, one of the primary amines was monoalkylated and the remaining one was protected with Fmoc-Cl. The final hydrolysis step yielded the corresponding Fmoc-cAzo AA (**1**).

The synthesis of peptide backbone switches would be more accessible if our molecular transducers were compatible with Fmoc solid-phase peptide synthesis (Fmoc-SPPS). However, the presence of halide substituents in the azobenzene derivatives makes them susceptible to aromatic nucleophilic substitution (S_NAr) under conventional Fmoc deprotection conditions (i.e., 20% piperidine/DMF).[20] Consequently, we envisioned using the 4-methyltrityl (Mtt) group[21] as an acid-labile amine protecting group because it is fully orthogonal to the side-chain ones. Thus, symmetrical dicarboxylic tetra-*ortho*-fluoroazobenzene (**9**)[18] was monofunctionalized at the *para* position through condensation with previously synthesized Mtt-protected ethylenediamine[22] under standard amidation conditions. This reaction provided **2** in moderate yields (Scheme 2).

Once the newly synthesized photoswitchable building blocks were characterized, with regard to purity and structural integrity (see the Supporting Information), they were incorporated into the peptide backbone of our previous PPI modulator, **3**, replacing the AMPB group. Synthesis of the cAzo peptide (**4**) was straightforward. On the contrary, extension of the peptide chain after inclusion of **2** required optimization. Thus, we explored mild deprotection methods for achieving efficient removal of the Fmoc group without affecting the integrity of the molecular transducer. As shown in Table 1, the use of a

Table 1. Conditions tested for mild Fmoc deprotection of a tetra-*ortho*-fluoroazobenzene-containing peptide on a solid support at 25 °C.

	Conditions	*t* [h]	Product	Starting material	Side products
A	50% Et_3N in CH_2Cl_2	17	✓	✓	✓
B	50% Bu_3N in CH_2Cl_2	17	✓	✓	✓
C	50% DIPEA in CH_2Cl_2	17	✓	✓	✓
D	20 mM NaOH in 30% dioxane/methanol	1.5	✓	×	✓
E	KF, [18]crown-6 in DMF	3	✓	✓	×
F	KF, [18]crown-6 in DMF	16	✓	×	×

few weaker, but more sterically hindered, bases than piperidine ($pK_a = 11.12$),[23] such as the tertiary amines *N*,*N*′-diisopropylethylamine (DIPEA; pK_a 10.75), triethylamine ($pK_a = 10.78$), and tributylamine ($pK_a = 10.89$), caused prolonged reaction times, incomplete conversion, and detectable chemical degradation (Figures S11 and S12 in the Supporting Information). Instead, complete deprotection was accomplished with a 20 mM solution of sodium hydroxide in 30% dioxane/MeOH after only 30 min.[24] Unfortunately, the reaction not only yielded the desired product, but also substitution side products (Figure S12, right). Likewise, other alternative conditions, such as piperazine

and 1,8-diazabicyclo[5.4.0]undec-7-ene (DBU) treatment, were previously discharged due to the detection of substitution side products with **9** (Figure S9). Only a solution of potassium fluoride (6.5 equiv) in DMF with catalytic amounts of [18]crown-6 provided the deprotection product neatly (Figure S13).[24] However, for time reasons, we resorted to peptide synthesis in solution through chemical ligation (see the Supporting Information) to obtain peptidomimetic **5** bearing the tetra-*ortho*-fluoroazobenzene derivative.

Photochemical behavior of photoswitchable peptidomimetics

Isomerization of the photoswitchable peptidomimetics **4** and **5** in aqueous solution was studied by means of UV–visible spectroscopy, HPLC, and NMR spectroscopy. A 0.128 mM solution of **4** prepared in the dark exhibited bands at $\lambda_{max}=295$ and 402 nm for the $\pi\rightarrow\pi^*$ and $n\rightarrow\pi^*$ transitions, respectively. This is consistent with the photochemical behavior of the *cis* unsubstituted parent cAzo.[8] Irradiation with a blue-light light-emitting diode (LED; $\lambda=405$ nm, see the Supporting Information for details) leads to spectroscopic changes in the solution: an increase of a band at $\lambda_{max}=475$ nm. Thus, in the photostationary state (PSS) at $\lambda=405$ nm, the $n\rightarrow\pi^*$ transition is shifted to longer wavelengths. The PSS was reached after just 1 s of irradiation (Figure S16). Importantly, there is a spectral region ($\lambda=500$–550 nm) where essentially only this isomer absorbs, which consequently enables quantitative *cis* isomerization under green LED irradiation ($\lambda=520$ nm; see the Supporting Information). Additional spectral changes were detected in the region of the $\pi\rightarrow\pi^*$ ($\lambda_{max}=295$ nm), where the absorption of the PSS at $\lambda=405$ nm was stronger than that of the PSS at $\lambda=520$ nm. Unlike the *trans* unsubstituted parental cAzo,[8] as well as the *trans*-4,4′- and 3,3′-*p*-acetamido-substituted ones,[9] no decrease of the band at $\lambda_{max}=402$ nm was observed in **4**, which was also observed in the 3,3′ polyurea-substituted analogues.[25] Upon irradiation with green light, the spectrum reverted to that of the thermodynamically favored *cis* isomer. In the case of **5**, the *trans* isomer was the most stable thermodynamically. Thus, a 0.105 mM solution of **5** prepared in the dark exhibited characteristic absorption bands of the *trans* tetra-*ortho*-fluoroazobenzene isomers:[7c] an intense band at $\lambda_{max}=319$ nm and a weaker one at $\lambda_{max}=457$ nm assigned to the $\pi\rightarrow\pi^*$ and $n\rightarrow\pi^*$ transitions, respectively. After 30 s of continuous irradiation with the green LED, the *cis* PSS was reached (Figure S15), which led to a drastic decrease of the band at $\lambda_{max}=319$ nm, a shift of the weaker band to shorter wavelengths ($\lambda_{max}=412$ nm), and an increase of a band at $\lambda_{max}=250$ nm. Irradiation at $\lambda=405$ nm reverted the spectrum to that of the *trans* isomer.

We next monitored the UV-visible absorptions of aqueous solutions of **4** and **5** after alternating irradiation cycles at $\lambda=405$ and 520 nm (Figure 1). We demonstrated the reversibility of photoisomerization (≥ 14 cycles) for our peptide backbone photoswitches without any signs of photodegradation and photochemical fatigue (Figure 1 B).

To determine both the ratio and stability of the isomers in the PSS, we used HPLC. In case of **5**, we integrated the peak area of the different chromatograms at the isosbestic point ($\lambda=275$ nm) and corroborated the isomer conversion ratio by means of ^{1}H NMR spectroscopy (Figure S19); for **4**, the HPLC chromatograms were recorded at $\lambda=395$ nm because both isomers exhibited the same intensity in absorption and, therefore, the same extinction coefficient. There was no clear isosbestic point. In both cases, the photoconversions were efficient with ratios over 85% for the corresponding isomers (Figure 1 C), except for the isomerization of peptidomimetic **4** upon irradiation with blue LEDs, for which only 16% of the *trans* isomer was detected at the PSS. This rather low conversion rate could be attributed to overlap of the $\pi\rightarrow\pi^*$ and $n\rightarrow\pi^*$ transitions in the *cis* isomer.[9a,25]

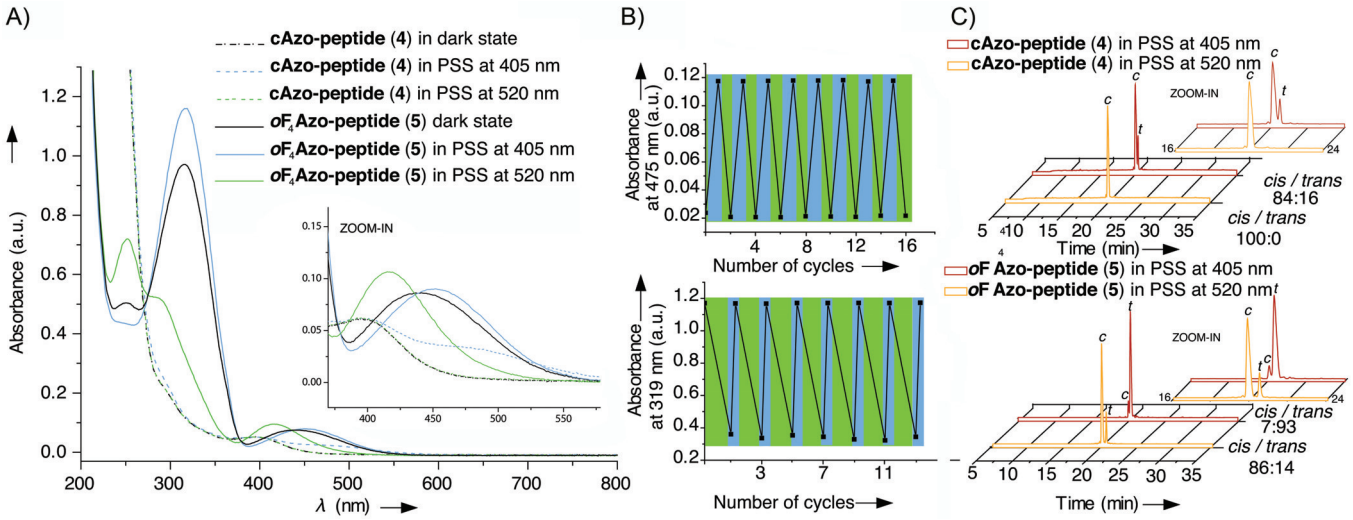

Figure 1. A) UV/Vis spectra of aqueous solutions of peptidomimetics **4** (0.128 mM; -----) or **5** (0.105 mM; ——) in the PSSs at $\lambda=405$ (blue) and 520 nm (green) at 25 °C. Inset: a magnification of the $\lambda=350$–600 nm region of the spectra. B) Reversible photochromism of **4** (top) and **5** (bottom) at $\lambda=475$ and 319 nm, respectively, upon alternating intervals of irradiation at $\lambda=405$ (blue) or 520 nm (green) at 25 °C. C) HPLC chromatograms and isomer ratios in the PSS at $\lambda=405$ (red) and 520 nm (orange) of **4** (top) and **5** (bottom) at 25 °C. Insets: magnifications of the region at 16–24 min.

Regarding the thermal stability, at room temperature, the isomer ratios at the PSSs are constant for at least 24 h in all cases, as long as the solutions are stored in total darkness (Figures S17 and S18). After 4 days, there is no dramatic change in isomer distribution, but side products are detected (< 8% in the PSS at $\lambda = 520$ nm of both compounds and in the PSS at $\lambda = 405$ nm of **5**; Figures S17 and S18). Interestingly, this degradation is more pronounced if the cAzo-containing peptide (**4**) is in the PSS at $\lambda = 405$ nm (*cis*/*trans* 84:16). The detected side products amounted to 29% and the substrate further degraded to 50% after one week (Figure S18). Nevertheless, stability for up to 3 days is compatible with the vast majority of biological assays.

Certain azobenzene derivatives are susceptible to reduction by intracellular thiols, whereas others are not. Glutathione (GSH) is the primary intracellular reducing agent, the expected highest intracellular concentration of which is 10 mM.[26] To have the possibility to use our compounds in a biological context, we evaluated the stability of both **4** and **5** in the presence of 10 mM GSH. Interestingly, the behavior of the peptidomimetics is different: whereas **5** was completely resistant to GSH reduction in both PSSs for 4 days (Figure S20), peptide **4** was found to be sensitive after just 1 day (Figure S21). This degradation effect was more severe in the PSS at $\lambda = 405$ nm, which was in agreement with our previous stability tests.

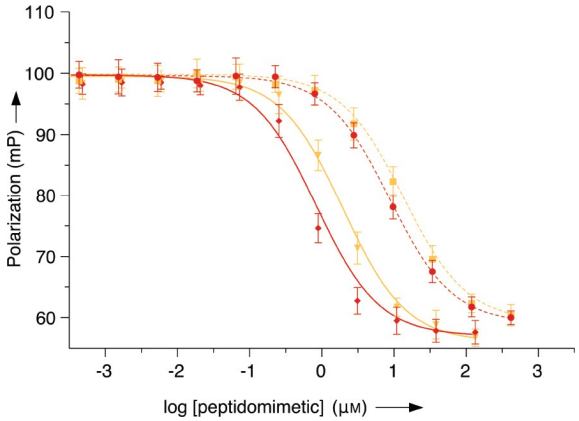

Figure 2. FP-based competitive assays of the peptidomimetics **4** (----) and **5** (——) in the PSSs at $\lambda = 405$ (● and ◆, respectively) and 520 nm (■ and ▼, respectively) at 25 °C. Mean data points and standard deviations are derived from three independent experiments.

Table 2. Binding affinities of the photoswitchable peptidomimetics to WDR5 at 25 °C.

Peptidomimetic	K_i [nM]		Ratio
	PSS at 405 nm	PSS at 520 nm	
4	140 ± 35	207 ± 52	1.5
5	11.8 ± 1.4	30.8 ± 3.3	2.6

Binding affinity of the photoswitchable peptidomimetics to WDR5 and inhibition of MLL1 activity

In our previous study, we demonstrated that the AMPB-containing peptide **3** was able to efficiently inhibit MLL1 activity through strong binding to the protein WDR5 (K_i in low-nM range for both isomers).[19] WDR5 belongs to the MLL1 protein core complex and is essential because WDR5 knockdown totally abolishes the histone methyltransferase (HMT) function of MLL1.[27] The newly synthesized peptidomimetics **4** and **5** are analogues of **3** bearing either the cAzo derivative or *o*F_4Azo, respectively. Thus, once these visible-light photoswitchable peptidomimetics were synthesized and photochemically characterized, we investigated their WDR5-binding capacities and possible differences between isomers. To this end, we used our previously optimized fluorescence polarization (FP) competitive assay,[19] with alteration to the irradiation step. We included the corresponding controls to rule out any interference with the isomerization (Figures S22–S25). The obtained results are summarized in Figure 2 and Table 2; the IC_{50} values (Table S1) were transformed into inhibition constants (K_i) to enable objective comparisons,[28] in particular, with our former peptide **3**.

All our novel peptidomimetics interacted with WDR5 with high affinity, in the nanomolar range (Table 2). In comparison with our previous results, peptide **3** proved to be the photoswitchable peptidomimetic with the highest affinity to WDR5, as well as the biggest difference between isomers ($K_i = 1.25$ nM for *trans*-**3**; $K_i = 6.50$ nM for *cis*-**3**; ratio: 5.0). Thus, exchange of the azobenzene with the cyclic analogue caused a more than 100-fold decrease in affinity to WDR5, relative to that with **3**, whereas, as expected, the incorporation of the small fluorine atoms into the azobenzene unit (**5**) affected the binding properties only slightly. Furthermore, the improved photoconversion properties of **5** were not directly translated into higher differences between isomers in our FP-binding assays compared with **3**. Nevertheless, it should be remembered that even low photoconversions can trigger significant biological effects. From all of our results so far, we selected **5** for further biological assays.

Next, we explored if visible-light photoswitchable peptidomimetic **5** could modulate the essential PPI of the MLL1 core complex (MLL1-WDR5) and, in turn, MLL1 activity. To this end and to avoid radioactivity, we used an amplified luminescent proximity homogeneous (AlphaLISA) assay[29] with the tetramer reconstituted MLL1 core complex (i.e., MLL1, WDR5, RbBP5, and Ash2L), the H3-21-mer peptide as a substrate, and the cofactor *S*-adenosyl methionine (SAM) as a universal methyl group donor. Gratifyingly, the functional data obtained from our AlphaLISA-based MLL HMT assay demonstrated that **5** effectively inhibited MLL1 activity (Figure 3; IC_{50} for *trans* **5** = (0.927 ± 0.034) μM, IC_{50} for *cis* **5** = (1.73 ± 0.12) μM) through disruption of the WDR5-MLL1 PPI due to its high affinity to WDR5. Notably, these determined potencies are based on the ability of **5** to inhibit the mono- and dimethylation function of the reconstituted MLL1 core complex. In addition, we could observe a modest, yet clear, difference between isomers of up to 1.8-fold. To further corroborate effective PPI disruption by **5** and the slight difference between isomers, we performed GST pull-down experiments. We incubated 0.262 μM GST-tagged MLL1 protein with the remaining proteins of the core complex to a final concentration of 0.4 μM. Afterwards, increasing

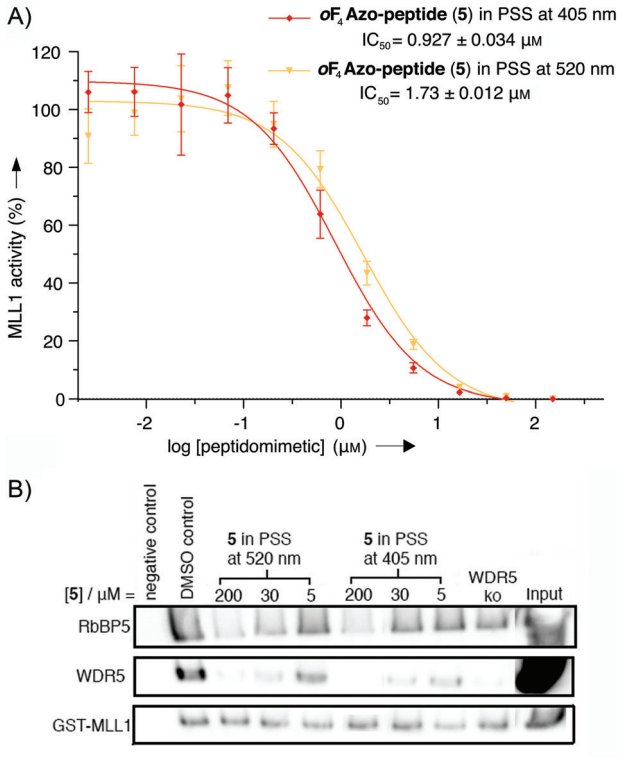

Figure 3. A) In vitro functional HMT AlphaLISA assay to evaluate the potency of peptidomimetic **5** to inhibit MLL1 enzymatic activity in the PSSs at $\lambda = 405$ (◆) and 520 nm (▼). Mean data points and standard deviations are derived from three independent experiments. B) In vitro glutathione–sepharose–transferase (GST) pull-down assay with the reconstituted 4-mer MLL1 core complex in the presence of **5** in the PSSs at $\lambda = 405$ and 520 nm; ko = knockout.

amounts of isomers of **5** were added. Both isomers were able to disrupt the MLL1 complex in a dose-dependent fashion. Importantly, we demonstrated different behavior between isomers: the *trans* isomer, again, showed a higher dissociation potential through its higher affinity to WDR5. These results are consistent with our FP-based experiments, as well as with the AlphaLISA-based MLL HMT assays. Therefore, collectively, our results confirm that visible-light irradiation triggers conformational changes in peptidomimetic **5**, which affect its capacity to modulate the WDR5-MLL1 PPI and, consequently, its potential to inhibit MLL1.

Crystal structure determination and structural basis of the peptidomimetic–WDR5 interaction

To understand the molecular principles behind the observed affinity deviations, we aimed to crystallize WDR5 in complex with peptidomimetics **4** and **5**. No crystals have been obtained for **5** in any PSS, to date. Cocrystallization with **4** in the PSS at $\lambda = 520$ nm (*cis* isomer) yielded crystals diffracting to a resolution of 1.51 Å (PDB ID: 6IAM).

The complex of WDR5 with **4** appears in a monoclinic crystal form (Table 3) that is distinct from those of previous crystal packings observed for WDR5–peptide complexes; this is most likely due to packing of the cAzo moiety against Pro168 of a

Table 3. Data collection and refinement of the cocrystal structure of WDR5 in complex with **4**.

Data collection	Values
λ [Å]	0.873 Å
resolution range [Å]	37.49–1.51 (1.564–1.51)
space group	$P12_11$
unit cell [Å,°]	$a = 46.53$, $b = 46.56$, $c = 66.17$, $\alpha = 90$, $\beta = 107$, $\gamma = 90$
total reflections	167527 (15726)
unique reflections	42377 (4073)
multiplicity	4.0 (3.9)
completeness (%)	99.3 (96.2)
mean $I/\sigma(I)$	9.04 (1.50)
Wilson B factor (Å^2)	11.27
R_{merge} [%]	0.0899 (0.713)
Refinement statistics	
R_{work}/R_{free} [%]	0.148/0.181
number of atoms	2895
protein	2377
ligands	100
solvent	418
protein residues	322
RMS (bonds/angles) [Å/°]	0.009/1.08
Ramachandran favored [%]	96.15
Ramachandran outliers [%]	0.00
rotamer outliers [%]	0.36
clashscore	2.20
average B factor [Å^2]	16.1
PDB ID	6IAM

symmetry-related complex. Nevertheless, the WDR5 structure is almost unaffected, with a low root-mean-square deviation (RMSD) of 0.200 Å for 262 Cα atoms upon superimposition on the WDR5–histone 3 peptide complex (PDB ID: 2CO0).[30] Peptide-bound WDR5 adopts the well-established β-propeller conformation, with a central cavity that accommodates the Arg3 side chain[31] that is part of the N-terminal recognition motif of **4**. The superimposition of **3** and **4** (Figure 4B) reveals almost identical interactions of the N-terminal stretches (SARA) with WDR5, including bridging water molecules and an α-helical main-chain trace. However, the central cAzo moiety packs differently to WDR5 than that of the linear azobenzene group of **3**. For example, the cAzo group lacks any direct interactions with the side chains of Lys259 and Tyr260, which are otherwise found for the WDR5–**3** complex. The C-terminal stretching of **4** (Val6–Ser11) is fully ordered, which might be due to interactions of the C-terminal carboxamide group with a symmetry-related WDR5 molecule, and adopts an α-helical conformation not observed previously for any cocrystals between WDR5 and MLL-derived peptides (Figure S26, right). Apart from additional packing interactions, peptide **4** establishes three water-mediated hydrogen bonds: the side-chain carbonyl group of Asp172 interacts with the backbone carbonyl group of Arg9 from the ligand. Likewise, the side-chain hydroxy group of Tyr191 and the amino group of the Lys259 coordinate a water molecule that bridges to the C-terminal backbone carbonyl of the cAzo entity (Figures S27 and S28).

We reported **3** to have an increased affinity in comparison to the WIN peptide (PDB ID: 3EG6) in a previous publication.[19]

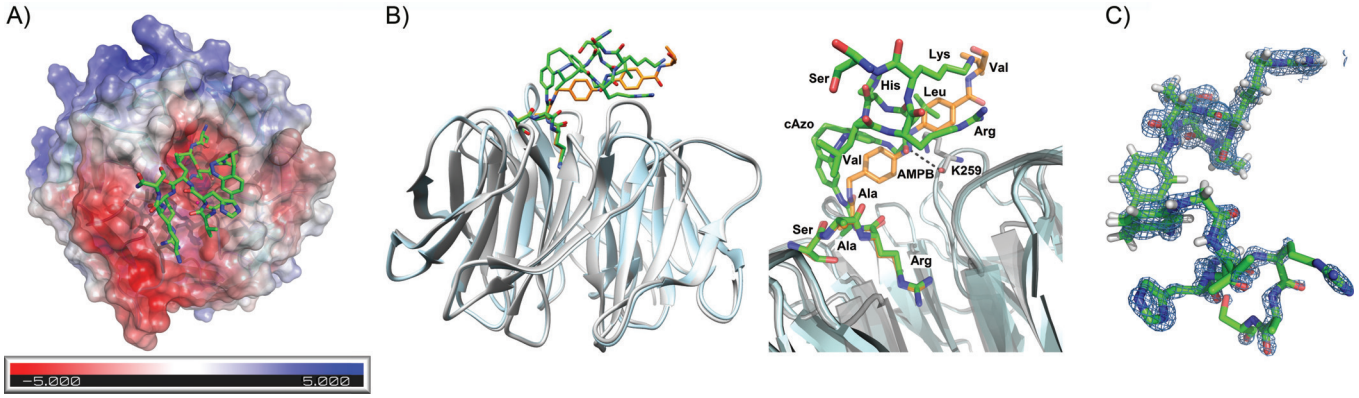

Figure 4. A) Crystal structure of WDR5 in complex with **4** (PDB ID: 6IAM); WDR5 is shown as a surface representation of its electrostatic potential with the color code from red (negative) to blue (positive) in dimensionless units of $k_B = T/e_c$, in which k_B is the Boltzmann constant, T is the temperature, and e_c is the charge of an electron (generated by using the APBS PyMOL plug-in). B) Left: side view of the superimposed cocrystal structures of **3** (orange) and **4** (green) to WDR5. Right: Close-up view of the left overlay B, in which the key hydrogen bond between **3** and WDR5 (K259) is highlighted, along with labeled residues and azobenzene motifs. C) The $2F_o - F_c$ experimental electron density map contoured at 1.0σ (blue) shows the density for **4**.

Because **4** lacks several of the interactions of **3**, it is not surprising that it has a lower binding affinity, which is, indeed, more comparable to the WIN peptide than that to **3** ($K_i = 120$ nM for WIN peptide; $K_i = 140$ nM for *cis*-**4**, and $K_i = 1.25$ nM for *trans*-**3**)

Molecular modeling of peptidomimetics–WDR5 interactions

To further rationalize the obtained experimental results and to set up a workflow for further design of novel photoswitchable peptidomimetics, a series of virtual docking (VD) and molecular dynamics (MD) calculations were performed.

For all six ligands, *cis/trans*-**3**, *cis/trans*-**4**, and *cis/trans*-**5**, initial poses for MD calculations were obtained through molecular docking. The docking protocol was validated with heavy atoms RMSD = 0.8915 calculated for the part of *trans*-**3** already resolved in the crystal structure (PDB ID: 5M23; Figure S29).[19] Considering the significant conformational flexibility of peptidomimetics, several initial protein–ligand complexes were generated for each ligand. Only protein–ligand complexes in which the N-terminal part of the peptidomimetics (SARA-) remained stabilized during 20 ns MD production runs were used for further analysis. Results of MD simulations expressed as RMSD fluctuations of the N-terminal part of peptidomimetics (SARA-; Figure 5), and the whole protein (Figure S30) during 20 ns of production runs indicate reasonably stabilized complexes converged to the equilibration state.

The molecular mechanics Poisson–Boltzmann surface area (MM/PBSA) calculations of the binding energy were performed on the last 7 ns of each simulation to further validate predicted binding modes of the peptidomimetics and to investigate the relationship between experimental K_i values (transformed in $pK_{i\ exptl} = -\log K_i$) derived for the synthesized photoswitchable peptidomimetics and their calculated MM/PBSA scores. A linear regression model with $R^2 = 0.88$ between aforementioned parameters was established (Table 4); thus indicating that this model could be used as a predictive tool with discriminative properties between *cis* and *trans* isomers for structurally similar peptidomimetics.

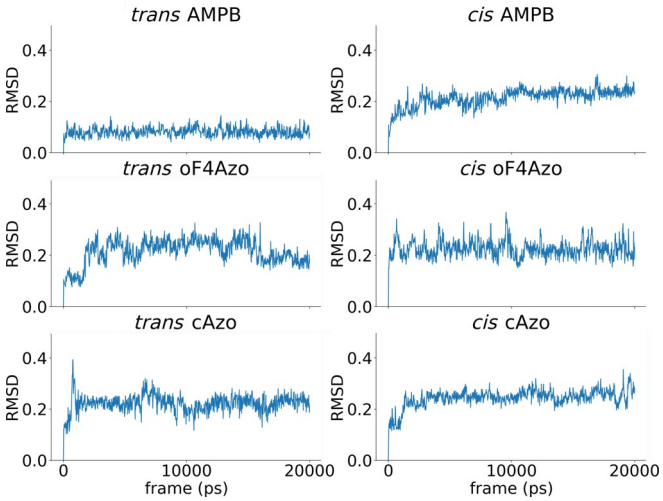

Figure 5. RMSD fluctuations during 20 ns of MD production runs calculated for the SARA- sequence of the ligands.

Table 4. Results obtained from MM/PBSA calculations and regression analyses.

Peptidomimetic	$pK_{i\ exptl}$[a]	MM/PBSA score [kJ mol]
trans-**3**	8.903	−51.282
cis-**3**	8.187	−21.136
trans-**4**	6.854	−5.909
cis-**4**	6.684	−5.680
trans-**5**	7.923	−28.388
cis-**5**	7.511	−15.371

[a] $pK_{i\ exptl} = -19.2458(MM/PBSA) + 126.4877$, $R^2 = 0.88$.

To gain an insight into details of the molecular interactions, after a trajectory clustering procedure, obtained cluster representatives were further analyzed. For all of the examined ligands, the largest fluctuations were detected in the C-terminal part of the peptidomimetics (-VHLRKS; Figure S31). These re-

sults are in accordance with the previously published crystal structure of the **3**–WDR5 complex (PDB ID: 5M23), for which the C-terminal part of the peptidomimetics (-VHLRKS) remain unresolved.

The binding mode of *trans*-**3** remained similar to the binding mode observed in the crystallographic structure (PDB ID: 5M23; Figure S32), which further supported our computational workflow. Better stabilization of the SARA- sequence of *trans*-**3** relative to the other ligands was confirmed through inspection of RMSD plots (Figure 5) and calculation standard deviations of RMSD over the 20 ns of MD simulations (Table S3). According to MD simulations of *trans*-**3**, valine, as the least fluctuating residue from the C terminus of the peptidomimetic (-VHLRKS; Figure S31), was recognized as an important residue for stabilization of the protein–ligand complex. Upon comparing poses of *cis*-**3** and *trans*-**3** (Figure 6), the N-terminal part of both peptidomimetics (SARA-) remained similar; the largest difference was in the orientation of the azobenzene part of the ligand, and consequently, in the C-terminal part (-VHLRKS).

The binding mode of *trans*-**5** remained similar to that of *trans*-**3** with regard to the N-terminal domain, as expected, whereas the tetra-*ortho*-fluoroazobenzene moiety was partially shifted relative to the azobenzene moiety of *trans*-**3** (Figure S33). Leucine within the C-terminal part (-VHLRKS) showed transient intramolecular interactions with the tetra-*ortho*-fluoroazobenzene moiety during MD simulations (Figures 7 A, S33, and S35). This particular intramolecular interaction was seen as the main reason for increased C-terminal valine fluctuations compared with the same valine from *trans*-**3** during MD simulations (Figure S31). Valine retained a similar binding mode inside the WDR5 binding site to that of *trans*-**3** (Figure S33). Nevertheless, the similar orientation and position of the C-terminal valine from *trans* peptides **3** and **5** indicate its importance in the overall stabilization of the protein–ligand complex.

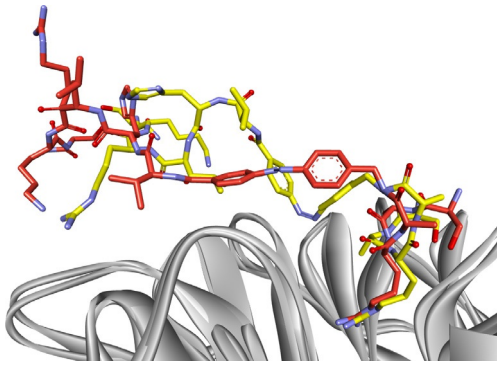

Figure 6. Difference in the binding modes obtained for *trans*-**3** (red) and *cis*-**3** (yellow) inside of the WDR5 binding site.

A significant shift in the binding conformation of the SARA-domain was observed for *cis*-**3** (Figure S35). Overall, the difference in observed binding modes between *cis/trans*-**3** and *cis/trans*-**5** can be interpreted as being due to different connectors between the SARA- domain and the novel fluorinated azobenzene. Thus, novel peptidomimetic **5** has a 2-aminoethyl-carbamoyl linker connecting the fluorinated azobenzene and SARA-domain, instead of the methylene group of peptidomimetic **3**, which connects the SARA- domain and unsubstituted azobenzene.

MD calculations performed for *trans*-**4** indicated that this isomer partially mimicked the positioning of other studied *trans* ligands (Figures 7 C and S36). The predicted MD binding mode of *cis*-**4** is comparable to that of its crystal structure (PDB ID: 6IAM) in terms of the orientation of the SARA-

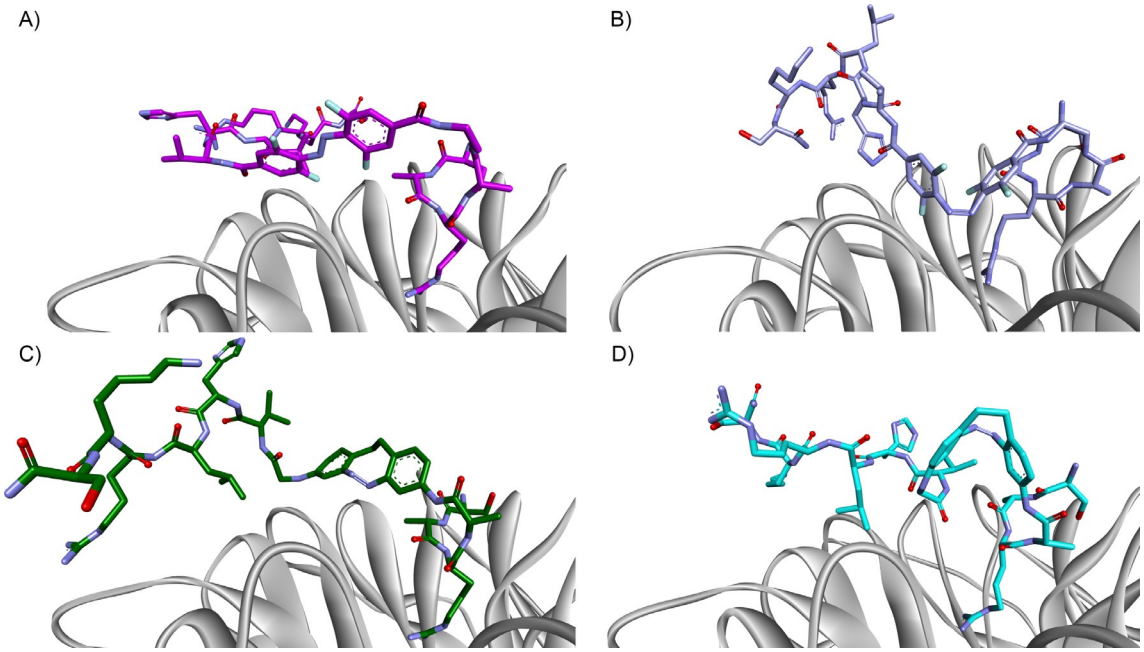

Figure 7. Binding modes of WDR5 and A) *trans*-**5** (dark purple); B) *cis*-**5** (light purple); C) *trans*-**4** (green), and D) *cis*-**4** (cyan).

sequence and cAzo moiety. This supports our computational workflow. However, some disagreement in the orientation of the -VHLRKS sequence was observed (Figure S37). Interestingly, as a part of the C-terminal -VHLRKS sequence, valine positioning in our crystal structure is comparable to the position of isoleucine of the predicted structure; thus signifying the importance of this region (residues Tyr131, Phe149) of the protein surface for the stabilization of a protein–ligand complex. Compared with *trans*-**4**, and to other ligands, the C-terminal part of *cis*-**4** interacted with a smaller part of the protein binding surface, which could be a partial explanation for the inability to crystalize protein–ligand complexes of the other peptides (Table S4).

The novel crystal structure of *cis*-**4** bound to WDR5, as well as linear regression derived for experimental results (pK_i values for the synthesized peptides) and MM/PBSA scores, makes this procedure promising for further in silico design of novel WDR5-MLL1 PPI photoswitchable disruptors. There is a need to design and synthesize novel derivatives of aforementioned peptidomimetics to increase the overall predictive power of such a computational study.

Conclusion

We have reported the synthesis of two visible-light photoswitchable amino acids for grafting onto a peptide scaffold. The goal was to use them as visible-light-responsive peptide backbone photoswitches and explore their potential as PPI modulators based on our former photoswitchable ligand **3**.[19] We found **5** particularly interesting because the only difference from the parental compound was the *ortho* incorporation of four fluorine atoms in the azobenzene motif and one additional methylene group in the linker of the azobenzene to alanine. Such modification improved the photochemical characteristics of this second-generation photoswitchable PPI modulator, which allowed better photoconversion under visible-light irradiation. This improvement, however, did not lead to a higher difference in the studied biological responses: neither in WDR5 affinity nor in MLL1 inhibition. This interesting observation highlights the difficulty in straightforwardly rationalizing the design of effective photoswitchable PPI inhibitors and plays down the quantitative photoconversion of the molecular transducer to achieve a functional binary system (on/off) in biological environments. For this purpose, having molecular information at our disposal is essential. Our structure–activity relationships determined from the novel crystal structure and computational methods shed light on binding to WDR5. The crystal structure and results from the molecular modeling study revealed substantial differences in the orientation of the azobenzene core for the characterized peptidomimetics. Agreement between experimental K_i values and MD results turns the developed in silico procedure into a promising tool for the further design of novel closely related peptidomimetics, which is our goal for further studies.

Although quantitative photoconversion of the photoswitches might not be essential for biological applications, visible-light irradiation is an indispensable requirement for in vivo use and to avoid phototoxicity. In addition, our photocontrollable peptide backbone switches offer benefits, such as fast isomerization and reversibility without degradation and high stability. Consequently, we believe that they will find applications in a wide range of light-driven molecular processes beyond protein control and related to photopharmacology, optobiology, materials science, antisense chemistry, or antimicrobial activity.

Experimental Section

General: All commercially reagents and solvents were purchased and used without further purification (see the Supporting Information). NMR spectra were recorded at 300 K on Bruker AV III HD 300 and 600 MHz spectrometers, whereas HRMS (ESI) results were acquired with a LTQ-FT Ultra mass spectrometer (Thermo Fischer Scientific), as specified in the Supporting Information.

Peptide synthesis: Peptides were synthesized according to the standard Fmoc-SPPS methodology and purified by means of preparative or semipreparative HPLC. Characterization was performed through HPLC-MS and HRMS (ESI). Peptide **5** was synthesized through the ligation reaction of two precursor peptides: Boc-S(*t*Bu)-A-R(Boc)$_2$-A-OH and H_2N-*o*F_4Azo-V-H(Trt)-L-R(Boc)$_2$-K(Boc)-S(*t*Bu)-$CONH_2$ (Boc: *tert*-butyloxycarbonyl, Trt: trityl).

Organic synthesis: Precursors **6** and **9** for the preparation of photoswitchable amino acids **1** and **2** were synthesized according to literature procedures.[8–9,32]

Compound 7: Compound **6** (200 mg, 0.840 mmol, 1.00 equiv) was dissolved in MeCN (4.26 mL), under a nitrogen atmosphere, and DIPEA (217 mg, 1.64 mmol, 2.00 equiv) was added to this solution. After the solution was heated to 60 °C, *tert*-butyl bromoacetate (163 mg, 0.84 mmol, 1.00 equiv) was added and stirred for 15 h. Afterwards, the solvent was removed under reduced pressure and the product was isolated by flash column chromatography (pentane/EtOAc 2:1). Product **7** was obtained as a yellow solid (107 mg, 0.304 mmol, 36%). TLC: R_f = 0.41 (pentane/EtOAc 1:1); ^{1}H NMR (300 MHz, $CDCl_3$): δ = 6.74 (t, ^3J = 8.2 Hz, 2H; 2×CH_{ar}), 6.32 (dd, ^3J = 8.1 Hz, ^4J = 2.4 Hz, 1H; CH_{ar}), 6.26 (dd, ^3J = 8.2 Hz, ^4J = 2.5 Hz, 1H; CH_{ar}), 6.13 (d, ^3J = 2.4 Hz, 1H; CH_{ar}), 6.02 (d, ^3J = 2.5 Hz, 1H; CH_{ar}), 4.20 (s, 1H; N*H*), 3.68 (s, 2H; $NHCH_2$), 3.57 (s, 2H; NH_2), 2.84–2.78 (m, 2H; CH_2), 2.61–2.55 (m, 2H; CH_2), 1.46 ppm (s, 9H; 3×CH_3); ^{13}C NMR (75 MHz, $CDCl_3$): δ = 170.1 (*CO*), 156.4 (C_{ar}), 156.3 (C_{ar}), 145.8 (C_{ar}), 144.9 (C_{ar}), 131.7 (C_{ar}H), 130.6 (C_{ar}H), 118.6 (C_{ar}), 117.8 (C_{ar}), 114.2 (C_{ar}H), 112.3 (C_{ar}H), 105.3 (C_{ar}H), 102.9 (C_{ar}H), 82.2 ($C(CH_3)_3$), 46.6 (CH_2NH), 31.2 (2×CH_2), 28.2 ppm (3×CH_3); HRMS (ESI+): *m/z* calcd for $C_{20}H_{24}N_4O_2H$ $[M+H]^+$: 353.1972; found: 353.1974.

Compound 8: Compound **7** (124 mg, 0.352 mmol, 1.00 equiv) dissolved in THF (2.30 mL) was cooled to 0 °C and pyridine (31.2 μL, 0.388 mmol, 1.10 equiv) was added. Then, Fmoc·Cl (100 mg, 0.288 mmol, 1.10 equiv) was added portionwise and the mixture was stirred at RT for 1.5 h. The mixture was diluted with 1 M HCl (2.0 mL), extracted with EtOAc (3×20.0 mL), washed with brine, and dried over anhydrous $MgSO_4$. The solvent was removed in vacuo. Product **8** was isolated by flash column chromatography (pentane/EtOAc 2:1) and obtained as a yellow solid (158 mg, 0.275 mmol, 78%). TLC: R_f = 0.47 (pentane/EtOAc 2:1); ^{1}H NMR (300 MHz, $CDCl_3$): δ = 7.77 (d, ^3J = 7.8 Hz, 2H; 2×CH_{ar}), 7.58 (d, ^3J = 7.3 Hz, 2H; 2×CH_{ar}), 7.41 (t, ^3J = 7.3 Hz, 2H; 2×CH_{ar}), 7.31 (td, ^3J = 7.4 Hz, ^4J = 1.0 Hz, 2H; 2×CH_{ar}), 6.92 (d, ^3J = 8.4 Hz, 1H; CH_{ar}), 6.78 (d, ^3J = 8.2 Hz, 1H; CH_{ar}), 6.63 (m, *1H;* CH_{ar}), 6.39 (dd, ^3J = 8.3 Hz,

^4J=2.4 Hz, 1H; CH_{ar}), 6.32–6.22 (m, 1H; CH_{ar}), 6.13 (d, ^3J=2.4 Hz, 1H; CH_{ar}), 4.51 (d, ^3J=6.4 Hz, 2H; OCH_2), 4.23 (t, ^3J=6.4 Hz, 1H; OCH$_2$CH), 3.67 (s, 2H; NHCH_2), 3.03–2.90 (m, 2H; CH_2), 2.90–2.68 (m, 2H; CH_2), 1.44 ppm (s, 9H; 3×CH_3); ^{13}C NMR (75 MHz, CDCl$_3$): δ=168.5(*C*O), 155.8 (*C*O), 143.8 (2×C_{ar}H), 141.4 (2×C_{ar}H), 136.7 (2×C_{ar}H), 130.5 (2×C_{ar}), 128.0 (2×C_{ar}), 127.7 (2×C_{ar}), 127.2 (2×C_{ar}), 127.1 (2×C_{ar}), 125.0 (2×C_{ar}), 124.9 (2×C_{ar}), 120.2 (2×C_{ar}), 120.1 (2×C_{ar}), 82.2 (*C*CH$_3$), 68.5 (*C*H$_2$), 52.9 (*C*H), 47.2 (*C*H$_2$), 31.9 (*C*H$_2$), 31.0 (*C*H$_2$), 28.2 ppm (3×*C*H$_3$); HRMS (ESI+): *m/z* calcd for $C_{35}H_{34}N_4O_4Na$ [*M*+Na]$^+$: 597.2472; found: 597.2473.

Compound 1: Compound **8** (202 mg, 0.352 mmol, 1.00 equiv) was dissolved in CH_2Cl_2 (2.50 mL) and cooled to 0 °C. Then TFA (5.00 mL) was added dropwise. After stirring for 10 h at RT, the solvent was removed under reduced pressure. The obtained residue was dissolved in EtOAc and water, extracted with EtOAc (3× 10.0 mL), and dried over anhydrous Na_2SO_4. The solvent was removed under reduced pressure and the product was isolated by flash column chromatography (CH_2Cl_2/MeOH 15:1). Product **1** was obtained as a yellow solid (85.8 mg, 0.165 mmol, 47%). TLC: R_f= 0.06 (CH_2Cl_2/MeOH 15:1); ^{1}H NMR (300 MHz, CDCl$_3$): δ=7.74 (d, ^3J=7.5 Hz, 2H; 2×CH_{ar}), 7.54 (d, ^3J=7.2 Hz, 2H; 2×CH_{ar}), 7.38 (t, ^3J=7.4 Hz, 2H; 2×CH_{ar}), 7.31–7.21 (m, 3H; 3×CH_{ar}), 6.82 (s, 2H; 2×CH_{ar}), 6.71 (d, ^3J=8.3 Hz, 1H; CH_{ar}), 6.21 (dd, ^3J=8.2 Hz, ^4J=2.4 Hz, 1H; CH_{ar}), 5.96 (t, ^3J=4.2 Hz, 1H; CH_{ar}), 4.48 (d, ^3J=6.4 Hz, 2H; OCH_2), 4.20 (d, ^3J=6.4 Hz, 1H; OCH$_2$CH), 3.74 (s, 2H; NHCH_2), 2.91–2.79 (m, 2H; CH_2), 2.67–2.54 ppm (m, 12H; CH_2); ^{13}C NMR (75 MHz, CDCl$_3$): δ=174.3 (*C*O), 156.2 (*C*O), 155.8 (2×C_{ar}), 145.6 (2×C_{ar}), 143.7 (2×C_{ar}), 141.5 (2×C_{ar}), 136.1 (C_{ar}), 130.8 (2×C_{ar}H), 130.4 (2×C_{ar}H), 128.0 (2×C_{ar}H), 127.3 (2×C_{ar}H), 125.0 (2×C_{ar}H), 120.2 (2×C_{ar}H), 118.2 (C_{ar}), 112.7 (C_{ar}H), 102.8 (C_{ar}H), 67.1 (CHCH$_2$), 47.2 (*C*HCH$_2$), 45.8 (NHCH$_2$), 31.3 (*C*H$_2$), 30.9 ppm (*C*H$_2$); HRMS (ESI+): *m/z* calcd for $C_{31}H_{26}N_4O_4H$ [*M*+H]$^+$: 519.2038; found: 519.2019.

Compound 2: Compound **9** (275. mg, 0.804 mmol, 1.50 equiv) was suspended in THF (20.0 mL). HATU (206 mg, 0.536 mmol, 1.00 equiv) and DIPEA (187 µL, 1.61 mmol, 2.00 equiv) were added and the resulting solution was stirred at RT. After 15 min, compound **10** (210 mg, 0.665 mmol, 1.20 equiv) in THF (7.00 mL) was added and the solution was stirred for 3 h at RT. Afterwards, the solvent was removed under reduced pressure and the crude product was purified by flash column chromatography (CH_2Cl_2/MeOH 45:1 +3% NEt$_3$) to yield the desired product **2** as the triethylamine salt as a red solid (244 mg, 0.329 mmol, 61%). To obtain the NMR spectra without traces of triethylamine, a small amount was further purified by flash column chromatography (MeCN/MeOH 45:1 +3% NH$_3$). TLC: R_f=0.16 (CH_2Cl_2/MeOH 45:1 +3% NEt$_3$); ^{1}H NMR (300 MHz, DMSO): δ=8.87 (s, 1H; CON*H*CH$_2$), 7.80 (d, ^3J=10.6 Hz, 4H; 4×CH_{ar}), 7.42 (d, ^3J=7.4 Hz, 4H; 4×CH_{ar}), 7.28 (t, ^3J=6.7 Hz, 6H; 6×CH_{ar}), 7.20 (d, ^3J=7.1 Hz, 2H; 2×CH_{ar}), 7.09 (d, ^3J=8.0 Hz, 2H; 2×CH_{ar}), 3.48–3.46 (m, 2H; CH_2NH), 2.26 (s, 3H; CH_3), 2.16 ppm (m, 2H; CH_2NH); ^{13}C NMR (75 MHz, DMSO): δ=164.5 (*C*O), 162.8 (*C*O), 156.1 (C_{ar}F), 155.9 (C_{ar}F), 152.6 (C_{ar}F), 152.4 (C_{ar}F), 150.3 (C_{ar}C), 146.1 (2×C_{ar}C), 144.0 (C_{ar}C), 142.9 (C_{ar}C), 138.7 (C_{ar}C), 135.7 (C_{ar}C), 135.0 (C_{ar}C), 128.3 (4×C_{ar}H), 128.2 (2×C_{ar}H), 127.6 (4×C_{ar}H), 127.5 (2×C_{ar}H), 125.9 (2×C_{ar}H), 113.9 (C_{ar}HCF), 113.6 (C_{ar}HCF), 112.2 (C_{ar}HCF), 111.9 (C_{ar}HCF), 82.4 (NHC*C*$_4$), 70.1 (NHCH$_2$), 43.1 (NHCH$_2$), 20.4 ppm (*C*H$_3$); HRMS (ESI+): *m/z* calcd for $C_{36}H_{27}F_4N_4O_3$ [*M*−H]$^-$: 639.2025; found: 639.2025.

UV/Vis spectroscopy and FP measurements: Concentration determinations, UV/Vis, and FP-based measurements were performed on a Tecan (Switzerland) Spark 20M multimode microplate reader at RT. All measurements for concentration determinations were performed in a 1400 µL quartz cuvette (Hellma Analytics (104F-QS) with a pathlength of 1 cm. FP assays were performed as described previously[19] in black 96-well microtiter plates (Greiner, ref. no. 655900) with excitation at λ=485 nm and emission at λ=530 nm. A detailed procedure of the FP-based assays is provided in the Supporting Information. K_i values were calculated by using the equation described previously by Wang et al. and the corresponding webpage provided by them.[28]

AlphaLISA HMT assay: The AlphaLISA HMT assay was performed in white 384-well plates (Corning, ref. no. 4512) and with the AlphaLISA buffer (50 mM Tris pH 8.0, 50 mM NaCl, 5 mM $MgSO_4$, 10% glycerol, 0.01% Tween-20, 1 mM dithiothreitol (DTT)). The MLL1 complex (MLL1, WDR5Δ23, Ash2L, RBbP5) was reconstituted in AlphaLISA buffer to obtain a 205 nM solution. Each reaction contained final concentrations of 100 nM MLL1 complex, 1.70 µM substrate H3-21-mer peptide (Anaspec), and 2.00 µM SAM (PerkinElmer). Both *trans* and *cis* isomers of peptidomimetic **5** (*trans*: previously irradiated at λ=405 nm for 5 min; *cis*: previously irradiated at λ=520 nm for 5 min, as discussed in the Supporting Information) were added at concentrations ranging from 1.70 nM to 150.0 µM and incubated with the preassembled MLL1 complex for 20 min on ice. Each plate contained triplicates of a negative DMSO biograde control, a positive control with the already methylated H3 peptide, and a blank with only buffer and DMSO. Reactions were initiated by the addition of the H3/SAM mixture and incubated for 3 h at RT, before addition of the acceptor and donor Alphabeads (equilibrated with the AlphaLISA buffers). After another 2 h of incubation at RT, luminescence was measured on a PerkinElmer EnVision plate reader (mirror: 444, emission: λ=570 nm). The experiment was performed in triplicate three times, independently.

GST pull-down assay: For the GST pull-down assay GST-tagged MLL1 (500 µL) in assay buffer (50 mM Tris, 150 mM NaCl, 1.00 mM phenylmethylsulfonyl fluoride (PMSF) protease inhibitor) with 0.05% NP-40 and 1×BSA were preincubated on a rotator with GSH-sepharose beads (20.0 µL; equilibrated with assay buffer) with a final concentration of 0.262 µM for 1.5 h at 4 °C. After three washing steps of the beads with lysis buffer (assay buffer +0.5% NP-40), the remaining proteins (WDR5Δ23, Ash2L, RbBP5) in assay buffer with 0.05% NP-40 and 1×BSA were added to the beads with a final concentration of 0.4 µM. After incubation for 5 min on ice, the respective concentrations (200, 30, 5 µM) of peptidomimetic **5** in DMSO (*cis* and *trans*: photoisomerization was performed as outlined in the Supporting Information) were added and the mixture was incubated on the rotator at 4 °C for 3 h. A negative control, to which no GST-MLL1 was added, and a positive DMSO biograde control were included in each assay. After 3 h, the beads were washed with lysis buffer (5×), incubated with SDS-loading dye (80 µL; 0.5 M Tris pH 6.8), 5% SDS, 25% glycerol, 5% bromophenol blue in MilliQ water), and the proteins were denatured by incubation at 95 °C for 5 min. After SDS-PAGE (12%, following a protocol of the *Lab FAQs* from Roche), the bound proteins were detected by means of immunoblots (Western blot buffers, following a protocol of the *Lab FAQs* from Roche and the *Western Blotting Protocol* (Tank Transfer) from Sigma Aldrich) by using appropriate antibodies (rabbit antibodies from Bethyl, USA: anti-MLL1 (A300-375A), anti-WDR5 (A302-429A), anti-RbBP5 (A300-109A)).

Crystallization, data collection, structure determination and analysis

Crystallization of WDR5Δ23–4 Complex: WDR5 was concentrated to 200 µM, mixed with 25.9 mM **4** to yield final concentrations of 194 µM protein and 792.5 µM **4** (ratio: 1:4 protein/peptide), and crystallized in SWISSCI MRC two-well crystallization plates (Jena

Bioscience). The reservoir solution volume was 50 μL, the drops contained 1 μL of a 1:1 mixture of protein and crystallization solution. Crystal growth took place at 4 °C in a solution containing 10% (*w*/*v*) poly(ethylene glycol) (PEG) 20000, 20% (*v*/*v*) PEG 550 monomethyl ether (MME), 0.02 M sodium formate, 0.02 M ammonium acetate, 0.02 M trisodium citrate, 0.02 M sodium potassium L-tartrate, and 0.02 M sodium oxamate. Crystals were obtained after 2 weeks and flash-cooled in liquid nitrogen without additional cryoprotectant. Diffraction data were collected at the European Synchrotron Radiation Facility (ESRF) by using beamline ID23-2 equipped with a microdiffractometer and Pilatus3×2M detector. The crystals diffracted to 1.51 Å with X-ray radiation of 14.2 keV (0.873 Å). The data were processed by using XDS[33] in space group $P12_11$. Data reduction and scaling were performed by using CCP4i2 (Version 7.0.065),[34] with AIMLESS (Version 0.7.3).[35] The phases were solved by molecular replacement with the previously determined structure of the WDR5 in complex with another peptidomimetic inhibitor (PDB ID: 5M23)[19] by using PHASER.[36] The model was built by using COOT (Version 0.8.9)[37] and refinement in PHENIX (Version 1.11.1)[38] until $R_{work}=16.7\%$ and $R_{free}=17.2\%$ were achieved. The peptidomimetic restraints were generated through ReadySet.[38] Final refinement statistics are given in Table 3. All structural representation were generated by using PyMOL (Version 2.2). The coordinates and structure factors have been deposited with the Protein Data Bank under PDB ID: 6IAM.

Molecular docking: For VD of ligands into WDR5, GOLD 5.6 software[39] was used. Docking of peptides as PPI inhibitors still represents a challenging task due to significant flexibility of peptides and challenges in identifications of hot-spot regions on protein surfaces.[40] Although there are spatialized algorithms for the docking of peptides, the GOLD algorithm, which is primarily intended for small-molecule docking, has proven to be accurate and a fast alternative,[41] especially in this particular case in which it is reasonable to assume that the ARA sequence retains a similar binding mode. Application of more specialized methodologies for peptide–protein docking was hampered by the fact that the photoswitch in our ligands was introduced in the middle of peptide sequence; thus making them unsuitable for these procedures. Exploiting the known SARA- sequence conformation obtained in PDB ID: 5M23, a docking procedure in GOLD was set in two steps, in which a fragment-based approach for molecular docking was employed. The docking protocol was set up in two steps: 1) Fragment SARA-Azo (Azo indicates azobenzenes/diazocines) was docked in PDB ID: 5M23 by using substructure constraints on the SARA- sequence. The SARA- sequence conformation was retained from the PDB structure, whereas Azo was manually added to the SARA- sequence and the final conformation for first docking was generated in a 20 ns MD run of this ligand with position restraints added to the SARA- sequence with Gromacs 5.1.4 software, as explained in more detail in the next section (MD calculations). 2) Docking of the whole molecule was performed by constraining the SARA-Azo-pose obtained in the previous docking step. The peptide fragment (-VHLRKS sequence) was built in DS Visualizer in the β-sheet conformation. The final conformation of the ligand VHLRKS sequence was generated after a 20 ns MD run of the ligand with position restraints added to the SARA- sequence, with the Gromacs 5.1.4 software, as explained in the next section (MD calculations). For molecular docking, the PLP scoring function was used, with 50 poses generated and maximum flexibility accounted for ligands. The binding site was selected as the area of 8 Å around the ligand. Constraint weights were 20 for the SARA- sequence and 5 for azobenzene. Only poses with the smallest RMSD of the SARA- sequence, relative to PDB ID: 5M23, were retained for further MD studies.

MD calculations: The MD protocol included a definition of azobenzenes as novel residues. Parameters for azobenzenes were obtained from the ParamChem web server[42] and manually included in the Charmm36 force-field.[43] Gromacs 5.1.4 software was used for all MD simulations. Protonation for protein–ligand complexes were determined with the PROPKA server.[44] The protein was parametrized by the CHARMM36 force field for the amino acids of the ligands. The water model employed was TIP3P and an octahedron simulation box was used. The solvated system was preliminarily minimized by 5000 steps of steepest descent. The system was then heated to 310 K during 250 ps in an NVT ensemble with 1 fs time steps. Subsequently, the pressure was equilibrated to 1 atm during the 500 ps NPT simulation with 2 fs time steps. In the equilibration steps, harmonic positional restraints were set on the backbone of the protein with a spring constant of 1000 $kJ\,mol^{-1}\,Å^{-2}$. The position restraints used in equilibration were gradually removed during 1 ns simulation with 2 fs time steps. The production run was performed in the NPT ensemble at 310 K without any restraint, except for simulations with ligands only where position restraints were kept on the -SARA- sequence. The Verlet cutoff scheme, the Nose–Hoover thermostat, the Parrinello–Rahman barostat, LINCS for constraints (all bonds with H atoms), and the particle mesh Ewald for electrostatics were applied. Upon completion of the simulation, a Gromos clustering process[45] on the MD trajectory and relevant cluster representatives were obtained. MD simulations were used for refinement of complexes generated by molecular docking. Only simulations in which the ARA sequence remained stable in the active site were retained for further MM/PBSA analyses.

MM/PBSA scoring: The MM/PBSA method was used for postprocessing of data generated from MD simulations. This method, as an end-point free energy calculation methodology, has been proven to be a useful tool for postprocessing results obtained by means of molecular docking followed by MD refinement.[46] Although this method is not accurate enough for the prediction of absolute binding free energies, mostly because MM/PBSA counts on severe thermodynamic approximations, it has been proven useful for the rationalization of experimental results on a series of similar ligands by ranking relative binding affinities.[46,47] Here, we used 20 ns production MD runs for the refinement of obtained docking poses, and the GMXPBSA 2.1 tool for the calculation of binding energies from every 18th snapshot extracted in the last 7 ns of simulations (total of 21 snapshots per trajectory) with the single-trajectory approach. The dielectric constant of the solute was switched to one, whereas all other parameters were retained on default values. The entopic term was neglected from calculations.

Acknowledgements

We gratefully acknowledge Prof. Dr. Eric Meggers for S1 laboratory accessibility; Norbert Frommknecht for design assistance and construction of the LED lamps. Numerical simulations were run on the PARADOX-IV supercomputing facility at the Scientific Computing Laboratory, National Center of Excellence for the Study of Complex Systems, Institute of Physics, Belgrade, supported, in part, by the Ministry of Education, Science, and Technological Development of the Republic of Serbia under project no. ON171017. N.Dj., D.R. and K.N. acknowledge project no. 172033 of the Minis-

try of Science and Technological Development of the Republic of Serbia. Finally, we thank COST action CM1406 (Epigenetic Chemical Biology EPICHEMBIO) for support.

Conflict of Interest

The authors declare no conflict of interest.

Keywords: azobenzenes · isomerization · peptidomimetics · photochemistry · protein–protein interactions

[1] a) L. Bonetta, *Nature* **2010**, *468*, 851 – 854; b) H. C. Lu, A. Fornili, F. Fraternali, *Expert Rev. Proteomics* **2013**, *10*, 511 – 520.
[2] a) D. E. Scott, A. R. Bayly, C. Abell, J. Skidmore, *Nat. Rev. Drug Discovery* **2016**, *15*, 533 – 550; b) S. Surade, T. L. Blundell, *Chem. Biol.* **2012**, *19*, 42 – 50.
[3] a) N. Sawyer, A. M. Watkins, P. S. Arora, *Acc. Chem. Res.* **2017**, *50*, 1313 – 1322; b) I. S. Moreira, O. Sensoy, *Curr. Top Med. Chem.* **2018**, *18*, 645 – 646; c) T. Berg, *Angew. Chem. Int. Ed.* **2003**, *42*, 2462 – 2481; *Angew. Chem.* **2003**, *115*, 2566 – 2586; d) S. Gul, K. Hadian, *Expert Opin. Drug Discovery* **2014**, *9*, 1393 – 1404; e) L. G. Milroy, T. N. Grossmann, S. Hennig, L. Brunsveld, C. Ottmann, *Chem. Rev.* **2014**, *114*, 4695 – 4748; f) J. A. Wells, C. L. McClendon, *Nature* **2007**, *450*, 1001 – 1009; g) D. C. Fry, *Methods Mol. Biol.* **2015**, *1278*, 93 – 106; h) L. C. Cesa, A. K. Mapp, J. E. Gestwicki, *Front. Bioeng. Biotechnol.* **2015**, *3*, 119.
[4] a) L. Nevola, E. Giralt, *Chem. Commun.* **2015**, *51*, 3302 – 3315; b) M. Pelay-Gimeno, A. Glas, O. Koch, T. N. Grossmann, *Angew. Chem. Int. Ed.* **2015**, *54*, 8896 – 8927; *Angew. Chem.* **2015**, *127*, 9022 – 9054; c) A. Barnard, K. Long, H. L. Martin, J. A. Miles, T. A. Edwards, D. C. Tomlinson, A. Macdonald, A. J. Wilson, *Angew. Chem. Int. Ed.* **2015**, *54*, 2960 – 2965; *Angew. Chem.* **2015**, *127*, 3003 – 3008; d) P. Wójcik, L. Berlicki, *Bioorg. Med. Chem. Lett.* **2016**, *26*, 707 – 713.
[5] a) R. J. Mart, R. K. Allemann, *Chem. Commun.* **2016**, *52*, 12262 – 12277; b) H. M. D. Bandara, S. C. Burdette, *Chem. Soc. Rev.* **2012**, *41*, 1809 – 1825.
[6] a) M. M. Lerch, M. J. Hansen, G. M. van Dam, W. Szymanski, B. L. Feringa, *Angew. Chem. Int. Ed.* **2016**, *55*, 10978 – 10999; *Angew. Chem.* **2016**, *128*, 11140 – 11163; b) J. Broichhagen, J. A. Frank, D. Trauner, *Acc. Chem. Res.* **2015**, *48*, 1947 – 1960; c) Z. B. Mehta, N. R. Johnston, M. S. Nguyen-Tu, J. Broichhagen, P. Schultz, D. P. Larner, I. Leclerc, D. Trauner, G. A. Rutter, D. J. Hodson, *Sci. Rep.* **2017**, *7*, 291; d) A. A. Beharry, G. A. Woolley, *Chem. Soc. Rev.* **2011**, *40*, 4422 – 4437.
[7] a) M. X. Dong, A. Babalhavaeji, S. Samanta, A. A. Beharry, G. A. Woolley, *Acc. Chem. Res.* **2015**, *48*, 2662 – 2670; b) H. A. Wegner, *Angew. Chem. Int. Ed.* **2012**, *51*, 4787 – 4788; *Angew. Chem.* **2012**, *124*, 4869 – 4871; c) C. Knie, M. Utecht, F. L. Zhao, H. Kulla, S. Kovalenko, A. M. Brouwer, P. Saalfrank, S. Hecht, D. Bleger, *Chem. Eur. J.* **2014**, *20*, 16492 – 16501; d) M. Wegener, M. J. Hansen, A. J. M. Driessen, W. Szymanski, B. Feringa, *J. Am. Chem. Soc.* **2017**, *139*, 17979 – 17986; e) Z. Pianowski, *Chem. Eur. J.* **2019**, https://doi.org/10.1002/chem.201805814.
[8] R. Siewertsen, H. Neumann, B. Buchheim-Stehn, R. Herges, C. Nather, F. Renth, F. Temps, *J. Am. Chem. Soc.* **2009**, *131*, 15594 – 15595.
[9] a) H. Sell, C. Nather, R. Herges, *Beilstein J. Org. Chem.* **2013**, *9*, 1 – 7; b) S. Samanta, C. Qin, A. J. Lough, G. A. Woolley, *Angew. Chem. Int. Ed.* **2012**, *51*, 6452 – 6455; *Angew. Chem.* **2012**, *124*, 6558 – 6561.
[10] A. A. Beharry, O. Sadovski, G. A. Woolley, *J. Am. Chem. Soc.* **2011**, *133*, 19684 – 19687.
[11] a) M. Cigl, A. Bubnov, M. Kaspar, F. Hampl, V. Hamplova, O. Pacherova, J. Svoboda, *J. Mater. Chem. C* **2016**, *4*, 5326 – 5333; b) J. Karcher, Z. L. Pianowski, *Chem. Eur. J.* **2018**, *24*, 11605 – 11610.
[12] J. Luo, S. Samanta, M. Convertino, N. V. Dokholyan, A. Deiters, *ChemBioChem* **2018**, *19*, 2178 – 2185.
[13] F. Eljabu, J. Dhruval, H. B. Yan, *Bioorg. Med. Chem. Lett.* **2015**, *25*, 5594 – 5596.
[14] D. C. Burns, F. Zhang, G. A. Woolley, *Nat. Protoc.* **2007**, *2*, 251 – 258.
[15] a) M. Bose, D. Groff, J. M. Xie, E. Brustad, P. G. Schultz, *J. Am. Chem. Soc.* **2006**, *128*, 388 – 389; b) A. A. John, C. P. Ramil, Y. L. Tian, G. Cheng, Q. Lin, *Org. Lett.* **2015**, *17*, 6258 – 6261.
[16] R. Behrendt, M. Schenk, H. J. Musiol, L. Moroder, *J. Pept. Sci.* **1999**, *5*, 519 – 529.
[17] L. Ulysse, J. Chmielewski, *Bioorg. Med. Chem. Lett.* **1994**, *4*, 2145 – 2146.
[18] D. Bléger, J. Schwarz, A. M. Brouwer, S. Hecht, *J. Am. Chem. Soc.* **2012**, *134*, 20597 – 20600.
[19] L. Albert, J. Xu, R. W. Wan, V. Srinivasan, Y. L. Dou, O. Vazquez, *Chem. Sci.* **2017**, *8*, 4612 – 4618.
[20] a) Z. Ahmed, A. Siiskonen, M. Virkki, A. Priimagi, *Chem. Commun.* **2017**, *53*, 12520 – 12523; b) M. D. Wendt, A. R. Kunzer, *Tetrahedron Lett.* **2010**, *51*, 641 – 644.
[21] B. Sax, F. Dick, R. Tanner, J. Gosteli, *Pept. Res.* **1992**, *5*, 245 – 246.
[22] D. Chouikhi, M. Ciobanu, C. Zambaldo, V. Duplan, S. Barluenga, N. Winssinger, *Chem. Eur. J.* **2012**, *18*, 12698 – 12704.
[23] K. Ralhan, V. G. KrishnaKumar, S. Gupta, *RSC Adv.* **2015**, *5*, 104417 – 104425.
[24] G. B. Fields, *Methods Mol. Biol.* **1994**, *35*, 17 – 27.
[25] S. Z. Li, G. Han, W. Q. Zhang, *Macromolecules* **2018**, *51*, 4290 – 4297.
[26] a) H. R. López-Mirabal, J. R. Winther, *Biochim. Biophys. Acta Mol. Cell Res.* **2008**, *1783*, 629 – 640; b) C. Boulègue, M. Loweneck, C. Renner, L. Moroder, *ChemBioChem* **2007**, *8*, 591 – 594.
[27] Y. Dou, T. A. Milne, A. J. Ruthenburg, S. Lee, J. W. Lee, G. L. Verdine, C. D. Allis, R. G. Roeder, *Nat. Struct. Mol. Biol.* **2006**, *13*, 713 – 719.
[28] Z. Nikolovska-Coleska, R. Wang, X. Fang, H. Pan, Y. Tomita, P. Li, P. P. Roller, K. Krajewski, N. G. Saito, J. A. Stuckey, S. Wang, *Anal. Biochem.* **2004**, *332*, 261 – 273.
[29] H. Karatas, Y. Li, L. Liu, J. Ji, S. Lee, Y. Chen, J. Yang, L. Huang, D. Bernard, J. Xu, E. C. Townsend, F. Cao, X. Ran, X. Li, B. Wen, D. Sun, J. A. Stuckey, M. Lei, Y. Dou, S. Wang, *J. Med. Chem.* **2017**, *60*, 4818 – 4839.
[30] A. J. Ruthenburg, W. Wang, D. M. Graybosch, H. Li, C. D. Allis, D. J. Patel, G. L. Verdine, *Nat. Struct. Mol. Biol.* **2006**, *13*, 704 – 712.
[31] a) N. L. Alicea-Velázquez, S. A. Shinsky, D. M. Loh, J. H. Lee, D. G. Skalnik, M. S. Cosgrove, *J. Biol. Chem.* **2016**, *291*, 22357 – 22372; b) J. J. Song, R. E. Kingston, *J. Biol. Chem.* **2008**, *283*, 35258 – 35264; c) A. Patel, V. Dharmarajan, M. S. Cosgrove, *J. Biol. Chem.* **2008**, *283*, 32158 – 32161.
[32] D. Bléger, S. Hecht, *Angew. Chem. Int. Ed.* **2015**, *54*, 11338 – 11349; *Angew. Chem.* **2015**, *127*, 11494 – 11506.
[33] W. Kabsch, *Acta Crystallogr. Sect. D Biol. Crystallogr.* **2010**, *66*, 125 – 132.
[34] M. D. Winn, C. C. Ballard, K. D. Cowtan, E. J. Dodson, P. Emsley, P. R. Evans, R. M. Keegan, E. B. Krissinel, A. G. Leslie, A. McCoy, S. J. McNicholas, G. N. Murshudov, N. S. Pannu, E. A. Potterton, H. R. Powell, R. J. Read, A. Vagin, K. S. Wilson, *Acta Crystallogr. Sect. D Biol. Crystallogr.* **2011**, *67*, 235 – 242.
[35] P. R. Evans, G. N. Murshudov, *Acta Crystallogr. Sect. D Biol. Crystallogr.* **2013**, *69*, 1204 – 1214.
[36] A. J. McCoy, R. W. Grosse-Kunstleve, P. D. Adams, M. D. Winn, L. C. Storoni, R. J. Read, *J. Appl. Crystallogr.* **2007**, *40*, 658 – 674.
[37] P. Emsley, B. Lohkamp, W. G. Scott, K. Cowtan, *Acta Crystallogr. Sect. D Biol. Crystallogr.* **2010**, *66*, 486 – 501.
[38] P. D. Adams, P. V. Afonine, G. Bunkoczi, V. B. Chen, I. W. Davis, N. Echols, J. J. Headd, L. W. Hung, G. J. Kapral, R. W. Grosse-Kunstleve, A. J. McCoy, N. W. Moriarty, R. Oeffner, R. J. Read, D. C. Richardson, J. S. Richardson, T. C. Terwilliger, P. H. Zwart, *Acta Crystallogr. Sect. D Biol. Crystallogr.* **2010**, *66*, 213 – 221.
[39] G. Jones, P. Willett, R. C. Glen, A. R. Leach, R. Taylor, *J. Mol. Biol.* **1997**, *267*, 727 – 748.
[40] M. Ciemny, M. Kurcinski, K. Kamel, A. Kolinski, N. Alam, O. Schueler-Furman, S. Kmiecik, *Drug Discovery Today* **2018**, *23*, 1530 – 1537.
[41] a) A. S. Hauser, B. Windshugel, *J. Chem. Inf. Model.* **2016**, *56*, 188 – 200; b) C. Lammi, C. Zanoni, G. Aiello, A. Arnoldi, G. Grazioso, *Sci. Rep.* **2016**, *6*, 29931.
[42] K. Vanommeslaeghe, E. Hatcher, C. Acharya, S. Kundu, S. Zhong, J. Shim, E. Darian, O. Guvench, P. Lopes, I. Vorobyov, A. D. Mackerell, Jr., *J Comput. Chem.* **2010**, *31*, 671 – 690.
[43] J. Huang, A. D. MacKerell, Jr., *J. Comput. Chem.* **2013**, *34*, 2135 – 2145.
[44] M. H. Olsson, C. R. Sondergaard, M. Rostkowski, J. H. Jensen, *J. Chem. Theory Comput.* **2011**, *7*, 525 – 537.

[45] X. Daura, K. Gademann, B. Jaun, D. Seebach, W. F. van Gunsteren, A. E. Mark, *Angew. Chem. Int. Ed.* **1999**, *38*, 236 – 240; *Angew. Chem.* **1999**, *111*, 249 – 253.

[46] T. Hou, J. Wang, Y. Li, W. Wang, *J. Chem. Inf. Model.* **2011**, *51*, 69 – 82.

[47] a) H. Y. Sun, Y. Y. Li, M. Y. Shen, S. Tian, L. Xu, P. C. Pan, Y. Guan, T. J. Hou, *Phys. Chem. Chem. Phys.* **2014**, *16*, 22035 – 22045; b) S. Genheden, U. Ryde, *Expert Opin. Drug Discovery* **2015**, *10*, 449 – 461.

Manuscript received: November 29, 2018

Accepted manuscript online: January 24, 2019

Version of record online: April 25, 2019